A variational approach for three-dimensional model of extensible marine cables with specified top tension

Somchai Chucheepsakul *, Narakorn Srinil, Pisek Petchpeart

Department of Civil Engineering, King Mongkut's University of Technology Thonburi, Bangmod, Toongkru, Bangkok 10140, Thailand

Abstract

This paper presents a variational model formulation that can be used for analyzing the three-dimensional steady-state behavior of an extensible marine cable. The virtual work-energy functional, which involves virtual strain energy due to a cable stretching, and virtual works done by the gravitational, inertial and external drag forces, is formulated. Euler–Lagrange's equations, obtained by considering the first variation of the functional, are identical to those obtained by equilibrating forces on a cable infinitesimal segment. Two mathematical simulations, namely, the finite element method and the shooting-optimization technique, are employed to solve and evaluate the problems. The numerical investigations are carried out for the case of a specified end tension, whereas the specified cable unstrained length case can be applied in the algorithm procedure. The validity of the present model and the influence of various geometrical parameters on the cable equilibrium configuration are demonstrated. The effects of cable extensibility and the omnidirectionality of current actions are presented and discussed.
© 2003 Elsevier Inc. All rights reserved.

Keywords: Mathematical simulation; Variational approach; Three-dimensional marine cable model; Extensible marine cables; Finite element method; Shooting-optimization method

1. Introduction

With the increases in deployment of cables in deep-ocean engineering, the determination of cable configurations as well as cable tensile forces has become the important parameters in the design process. As far as the hydrodynamic drag forces are concerned, the performance of marine

---

* Corresponding author. Tel.: +662-470-9146; fax: +662-427-9063.
E-mail address: somchai.chu@kmutt.ac.th (S. Chucheepsakul).

cables must be considered in three-dimensional space. Hence, to accomplish a fundamental understanding of cable behaviors, accurate three-dimensional modelling of cable should be fully accounted for in the analysis.

The research work by De Zoysa [1] on the three-dimensional steady-state analysis of under cable towing a sea buggy was recognized by a number of researchers in the past. In that paper the static equilibrium equations of the problem are solved by using a shooting method. The obtained results showed the variations of tension components at the buggy end with respect to different directions made by the currents. Chucheepsakul and Subwonglee [2] solved the same problem using a variational approach. Wang et al. [3] used the shooting-optimization technique to yield more accuracy of the results. Friswell [4] corrected the hydrodynamic force model used by Wang et al. [3] and suggested approximate guidelines on choosing optimum cable length in the operating systems, in addition to the cable profile and tensile force developments. All of the aforementioned studies, however, do not take into consideration the effect of axial extensibility, which is essential for determining the cable configuration. This restriction may not yield an accurate analysis, especially in the case of cables having high extensibility.

Recently, a various of mathematical models of extensible cables has been considered by many researchers. A brief review of their work should be mentioned herein. Webster [5] presented the finite element approach to simulate the non-linear effects under hydrodynamic actions. Huyse et al. [6] modified the riser model to a three-dimensional tensioned string and used the cylindrical coordinates to obtain the admissible configuration. Dreyer and Van Vuuren [7] derived the numerical solutions of both continuous and discrete models through the concept of inextensible cable (elastic modulus is assumed to be large). Vassalos [8] provided detailed information on explaining the appropriate models in the design of marine structure. However, the essential parameters associated with the static behavior have not been tackled rigorously in their study [5–8]. Vaz and Patel [9] were particularly interested in investigating the cable configuration during installation in sheared current field. They demonstrated the importance of current profile for predicting of suspended line behaviors, especially when imposing a more complex three-dimensional current profile. Nevertheless, the influence of cable extensibility has not yet been thoroughly investigated. Thus, it is the main objective of this study to examine the geometrical parameters for any cable equilibrium configuration by including the extensibility effect under the omnidirectionality of the current actions. The important factors in the preliminary design stage include the cable tension distribution, elongation and geometric relations, such as cable unstrained or strained arc-length, vertical and horizontal angles of any point along a cable.

In the present paper numerical computations based on the finite element approach are used. The numerical technique presented in this study is computationally efficient to carry out for the solution in which the top tension is specified. However, the technique is not limited to the solution in which the total arc-length of cable is specified. A more detail description of this technique for two-dimensional case can be found in Chucheepsakul et al. [10]. As an alternative check, the shooting method is also used to validate the numerical solutions obtained from the variational approach.

The following assumptions are made throughout this analysis:

(1) A cable is installed with two stationary supports at the bottom and top end positions. Each end is held by the pinned support.

(2) The effect of bending, shear and torsional rigidities is neglected.
(3) The material of cable is assumed to be linearly elastic and the material density per unit volume remains invariant during stretching.

Numerical results are demonstrated tabularly and graphically for two case studies, namely, the practical cases of specified top tension and specified cable unstrained arc-length.

2. Cable model and governing equations

A typical cable model in its relationship to a fixed Cartesian reference frame called the global coordinate system is represented in Fig. 1a, which also shows the rotated system, i.e., the local coordinate system. This system is useful since it allows a simplified expression of the equations. The geometric compatibility relation of both systems can be expressed as the following matrix notation,

$$
\left\{ \begin{array}{c} \vec{i} \\ \vec{j} \\ \vec{k} \end{array} \right\} = \begin{bmatrix} \cos\phi\cos\theta & -\sin\theta & -\sin\phi\cos\theta \\ \cos\phi\sin\theta & \cos\theta & -\sin\phi\sin\theta \\ \sin\phi & 0 & \cos\phi \end{bmatrix} \left\{ \begin{array}{c} \vec{p} \\ \vec{q} \\ \vec{r} \end{array} \right\} \tag{1}
$$

in which unit vectors $\vec{i}, \vec{j}, \vec{k}$ and $\vec{p}, \vec{q}, \vec{r}$ represent for the sets of global and local coordinate systems, respectively. The cable orientation at any point is defined by ϕ and θ, where ϕ is the vertical angle between the XY plane and vector $\vec{p}$, θ is the horizontal angle between the XZ plane and projection line of vector $\vec{p}$, when vector $\vec{q}$ lies on the XY plane. The bottom end of the cable is anchored at the seabed, while the top end is tied to the floating structure. With regard to Fig. 1b, it can be seen the circular plan view of the cable configuration, in which θ_0 is the horizontal angle between X-axis and the projection line of cable chord length on XY plane, R is the distance along the seabed between the top and bottom ends.

The current velocity is a function of depth only and is given by $\vec{V} = v_x(z_0)\vec{i} + v_y(z_0)\vec{j}$. In terms of the local coordinate system, the current profile is taken as $\vec{V} = p_s\vec{p} + q_s\vec{q} + r_s\vec{r}$, namely

$$
p_s = v_x(z_0)\cos\phi\cos\theta + v_y(z_0)\cos\phi\sin\theta \tag{2a}
$$

$$
q_s = -v_x(z_0)\sin\theta + v_y(z_0)\cos\theta \tag{2b}
$$

$$
r_s = -v_x(z_0)\sin\phi\cos\theta - v_y(z_0)\sin\phi\sin\theta \tag{2c}
$$

For stationary cable, the drag force is given by $D_F = D_p\vec{p} + D_q\vec{q} + D_r\vec{r}$, in which D_p, D_q and D_r are the components of drag force along the direction of vectors $\vec{p}$, $\vec{q}$ and $\vec{r}$, respectively. Simple time-independent hydrodynamic loading models are chosen here, where the tangential and normal forces are proportional to the square of tangential and normal fluid velocities. Thus, D_F becomes

$$
D_F = C_\mathrm{T}p_s|p_s|\vec{p} + C_\mathrm{N}(q_s\cdot\vec{q} + r_s\cdot\vec{r})\sqrt{q_s^2 + r_s^2} \tag{3}
$$

$$
C_\mathrm{T} = \tfrac{1}{2}\rho_\mathrm{w}D\pi C_\mathrm{DT}(1 - v\varepsilon_0) \quad \text{and} \quad C_\mathrm{N} = \tfrac{1}{2}\rho_\mathrm{w}DC_\mathrm{DN}(1 - v\varepsilon_0) \tag{4a,b}
$$

in which ρ_w is the density of seawater, C_DT and C_DN are the tangential and normal drag coefficients, $D(1 - v\varepsilon_0)$ is the deformed cable diameter, and v is the Poisson's ratio.
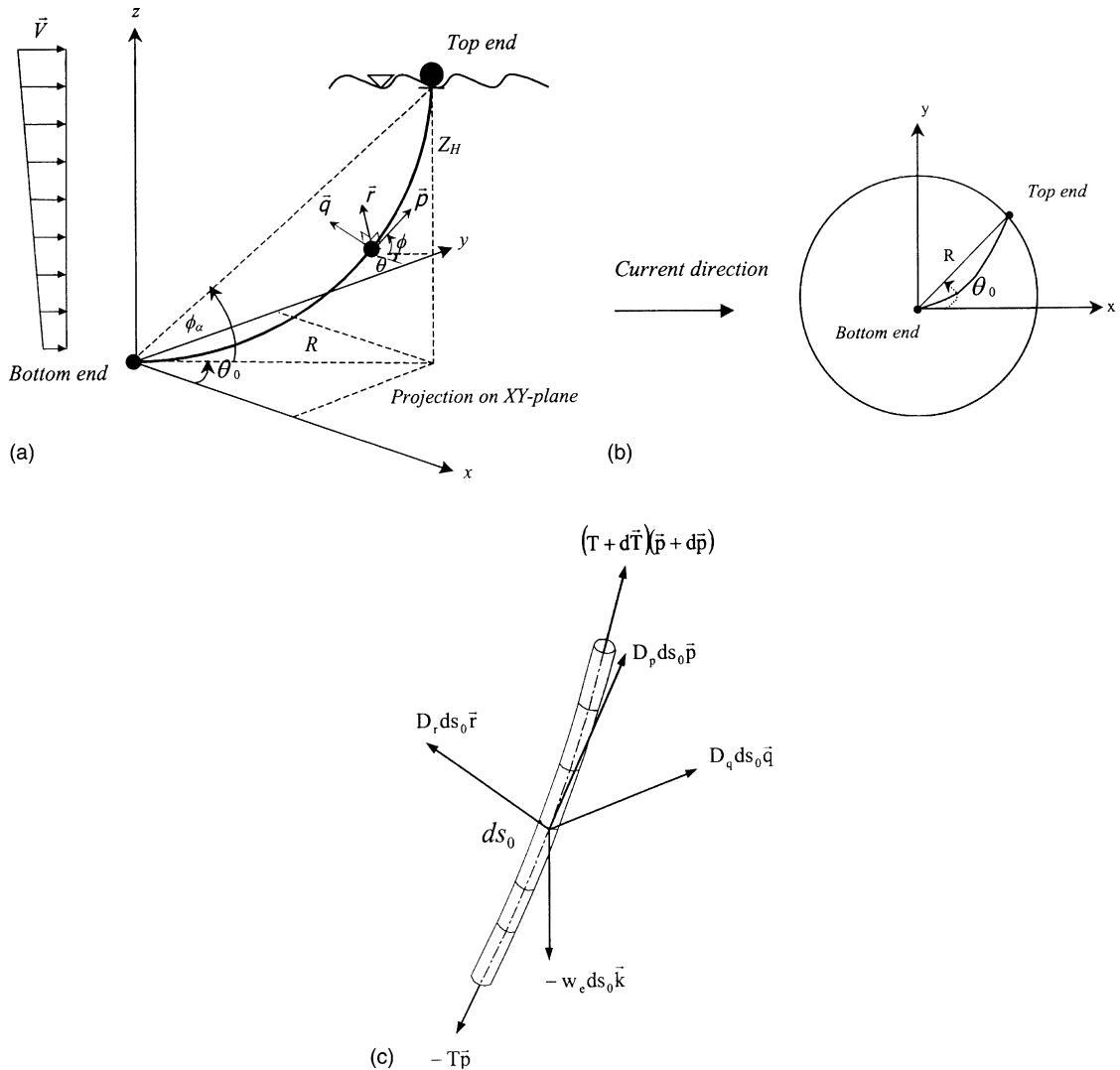
Fig. 1. (a) Reference configuration and coordinate systems of marine cables. (b) Circular plan view of cable model. (c) Forces on cable infinitesimal segment.

Referring to Fig. 1c, the equilibrium equations for an infinitesimal element of an immersed cable as given by Berteaux [11] can be written along the direction of $\vec{p}$, $\vec{q}$, $\vec{r}$ as

$$\frac{\mathrm{d}T}{\mathrm{d}s_0} = \frac{w_e \sin \phi}{(1 + \varepsilon_0)} - D_p$$

$$\frac{\mathrm{d}\theta}{\mathrm{d}s_0} = -\frac{D_q}{T \cos \phi}$$

$$\frac{\mathrm{d}\phi}{\mathrm{d}s_0} = \left(\frac{w_e \cos \phi}{(1 + \varepsilon_0)} - D_r \right) \bigg/ T$$

(5a,b,c)

where T is the cable effective tension and not the actual tension that controls the extensibility of the cable. The effective tension [12] is written as

$$T = EA\varepsilon_0 + 2v\rho_w gA(1 - v\varepsilon_0)^2(Z_H - z_0) \tag{6}$$

3. Variational formulation

Fig. 2 shows an infinitesimal element of cable in which u, v and w are the components of displacement from the equilibrium position in the direction of unit vectors $\vec{i}, \vec{j}, \vec{k}$, respectively. The derivatives of its length ds_0 in each direction are

$$dx_0 = \cos\phi\cos\theta\,ds_0, \quad dy_0 = \cos\phi\sin\theta\,ds_0 \quad \text{and} \quad dz_0 = \sin\phi\,ds_0 \tag{7a,b,c}$$

Differentiation of Eq. (7) with respect to z_0 ($'$), the cable stretched length is

$$ds_0 = \sqrt{1 + x_0'^2 + y_0'^2}\,dz_0 \tag{8}$$

Let $\sqrt{1 + x_0'^2 + y_0'^2}$ be s_0'. Another form of ds_0 using the Lagrangian strain definition is

$$ds_0 = (1 + \varepsilon_0)\,ds \tag{9a}$$

Thus,

$$ds = \frac{s_0'}{1 + \varepsilon_0}\,dz_0 \tag{9b}$$

in which ds is the unstretched cable length. Likewise, the arc-length $d\bar{s}$, the strain $\bar{\varepsilon}$ and the displacements u, v and w at the displaced state are given by

$$d\bar{s} = \sqrt{(x_0' + u')^2 + (y_0' + v')^2 + (1 + w')^2}\,dz_0 \tag{10a}$$

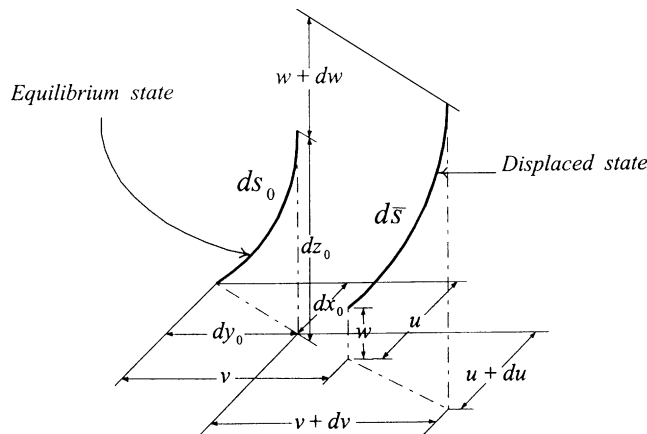$$d\bar{s} = (1 + \bar{\varepsilon})\,ds \tag{10b}$$

Fig. 2. Two different states of cables.

From Eqs. (8)–(10), one can write the dynamic strain as

$$\bar{\varepsilon} = \frac{d\bar{s} - ds}{ds} = \frac{1 + \varepsilon_0}{s_0'} \sqrt{(x_0' + u')^2 + (y_0' + v')^2 + (1 + w')^2} - 1 \tag{11}$$

and its variation can be written as

$$\delta\bar{\varepsilon} = \frac{1 + \varepsilon_0}{s_0'} \left[\frac{(x_0' + u')\delta u' + (y_0' + v')\delta v' + (1 + w')\delta w'}{\sqrt{(x_0' + u')^2 + (y_0' + v')^2 + (1 + w')^2}} \right] \tag{12}$$

3.1. Strain energy due to axial deformation

The strain energy due to axial deformation is caused by two actions, namely, pulling on the cable due to tension and the squeezing of the cable due to hydrostatic pressure, as proposed by Sparks [13]. The strain energy expression is written as

$$U = \int_0^{S_t} \frac{1}{2} EA\bar{\varepsilon}^2 \, ds + \int_0^{\bar{S}_t} 2v\rho_w gA_0(Z_H - z_0) \, d\bar{s} \tag{13}$$

where S_t is the total undeformed arc-length, $\bar{S}_t$ is the total deformed arc-length, E is Young's modulus, A and A_0 is the undeformed and deformed cable cross-sectional areas respectively. Using Eqs. (9), (11) and (12), the variation of Eq. (13) becomes

$$\delta U = \int_0^{Z_H} \left\{ \left[T_a + T_b \left(1 - \frac{1}{\sqrt{1 + 2\lambda}} \right) \right] \left[\frac{(x_0' + u')\delta u' + (y_0' + v')\delta v' + (1 + w')\delta w'}{s_0'} \right] \right\} dz_0 \tag{14}$$

$$\lambda = \frac{x_0'u' + y_0'v' + w' + \frac{1}{2}(u'^2 + v'^2 + w'^2)}{s_0'^2} \tag{15}$$

in which $T_a = EA\varepsilon_0 + 2v\rho_w gA_0(Z_H - z_0)$ and $T_b = EA - 2v\rho_w gA_0(Z_H - z_0)$, when Z_H is the total sea depth. It is seen that Eq. (6) and T_a are identical to the usual form of the cable effective tension. If Poisson's ratio v is set to be zero so that there is no reduction in cable diameter, then T_a is equal to the cable actual tension and axial strain is proportional to this tension [14]. By neglecting the small quantities of higher order terms, and using the binomial approximation, Eq. (15) reduces to

$$\lambda \cong \frac{x_0'u' + y_0'v' + w'}{s_0'^2} \quad \text{and} \quad \frac{1}{\sqrt{1 + 2\lambda}} \cong 1 - \lambda \tag{16a,b}$$

Substituting Eq. (16) into Eq. (14) yields

$$\begin{aligned}
\delta U = \int_0^{Z_H} &\left\{ \left[\frac{T_a}{s_0'}(x_0' + u') + \frac{T_b}{s_0'^3}(x_0'^2 u' + x_0'y_0'v' + x_0'w') \right] \delta u' \right. \\
&+ \left[\frac{T_a}{s_0'}(y_0' + v') + \frac{T_b}{s_0'^3}(x_0'y_0'u' + y_0'^2 v' + y_0'w') \right] \delta v' \\
&\left. + \left[\frac{T_a}{s_0'}(1 + w') + \frac{T_b}{s_0'^3}(x_0'u' + y_0'v' + w') \right] \delta w' \right\} dz_0
\end{aligned} \tag{17}$$

3.2. Virtual work done by external forces

The virtual work done by effective weight of a submerged cable is expressed as

$$\delta W_e = -\int_0^{Z_H} \frac{w_e s_0'}{1 + \varepsilon_0} \delta w \, dz_0 \tag{18}$$

where w_e is the effective weight of the cable.

The virtual work done by hydrodynamic forces is written as

$$\delta W_H = \int_0^{Z_H} s_0'[(D_{pu} + D_{qu} + D_{ru})\delta u + (D_{pv} + D_{qv} + D_{rv})\delta v + (D_{pw} + D_{qw} + D_{rw})\delta w]dz_0 \tag{19}$$

in which the subscripts u, v and w denote the forces per unit length components corresponding to the Cartesian system.

The virtual work done by inertia force is

$$\delta W_i = -\int_0^{Z_H} (\bar{m}\ddot{u}\,\delta u + \bar{m}\ddot{v}\,\delta v + \bar{m}\ddot{w}\,\delta w)dz_0 \tag{20}$$

where $\bar{m} = (w_C/g(1 + \varepsilon_0))s_0'$ is the cable mass per unit stretched length at the equilibrium state, and w_C is the cable weight per unit unstretched length.

3.3. Euler's equations

The virtual work-energy of the marine cable system is written as

$$\delta \Pi = \delta U - \delta W_e - \delta W_H - \delta W_i = 0 \tag{21}$$

Substitution of Eqs. (17)–(20) into Eq. (21), then integration by part of Eq. (21) is performed by evaluating $\delta u = \delta v = \delta w = 0$ at boundary conditions, i.e., $z_0 = 0$ and $z_0 = Z_H$. Then, Euler's equations associated with the virtual displacement δu, δv and δw are obtained respectively as

$$\left[\frac{T_a}{s_0'}(x_0' + u') + \frac{T_b}{s_0'^3}(x_0'^2 u' + x_0' y_0' v' + x_0' w')\right]' - \bar{m}\ddot{u} = -(D_{pu} + D_{qu} + D_{ru})s_0' \tag{22}$$

$$\left[\frac{T_a}{s_0'}(y_0' + v') + \frac{T_b}{s_0'^3}(x_0' y_0' u' + y_0'^2 v' + y_0' w')\right]' - \bar{m}\ddot{v} = -(D_{pv} + D_{qv} + D_{rv})s_0' \tag{23}$$

$$\left[\frac{T_a}{s_0'}(1 + w') + \frac{T_b}{s_0'^3}(x_0' u' + y_0' v' + w')\right]' - \bar{m}\ddot{w} = -\left(D_{pw} + D_{qw} + D_{rw} - \frac{w_e}{1 + \varepsilon_0}\right)s_0' \tag{24}$$

3.4. Equilibrium equations

Applying the initial conditions $u = v = w = u' = v' = w' = u'' = v'' = w'' = \ddot{u} = \ddot{v} = \ddot{w} = 0$ on Eqs. (22)–(24), the following equilibrium equations are obtained

$$\left(\frac{T_a x_0'}{s_0'}\right)' + (D_{pu} + D_{qu} + D_{ru})s_0' = 0 \tag{25}$$

$$\left(\frac{T_a y_0'}{s_0'}\right)' + (D_{pv} + D_{qv} + D_{rv})s_0' = 0 \tag{26}$$

$$\left(\frac{T_a}{s_0'}\right)' + \left(D_{pw} + D_{qw} + D_{rw} - \frac{w_e}{1 + \varepsilon_0}\right)s_0' = 0 \tag{27}$$

It is noted that when assembling these equations using vector relations yields the equilibrium equation, which is identical to Eq. (5).

4. Mathematical simulations

Eqs. (25)–(27) are the system of non-linear differential equations, analytical solution to these equations are not be obtainable. Numerical solutions using the finite element method or the shooting-optimization may be used for practical problems. For the purposes of comparison and validation of the results, the two numerical methods are employed in this investigation. In the finite element procedure, the variational formulation given in Eqs. (17)–(21) is involved while in the shooting-optimization method the governing differential equation given in Eqs. (5) is used. In each method, either top tension or the cable unstrained arc-length may be either known a prior or may be determined.

4.1. Finite element method

For independent variable z_0, only the variation of horizontal displacement is considered, $\delta w = \delta w' = 0$. The reference of three-dimensional equilibrium configuration is determined by substitution of Eqs. (17)–(20) into Eq. (21) again, and then Eq. (21) is rearranged in the form of a hybrid formulation as follows

$$\delta \Pi = \delta \int_0^{Z_H} \left[T_a \sqrt{1 + (x_0' + u')^2 + (y_0' + v')^2} - F_u s_0' u - F_v s_0' v \right] dz_0 = 0 \tag{28}$$

in which $F_u = D_{pu} + D_{qu} + D_{ru}$ and $F_v = D_{pv} + D_{qv} + D_{rv}$. At the displaced state, $x = x_0 + u$, $y = y_0 + v$, hence $x' = x_0' + u'$, $\delta x = \delta u$, $\delta x' = \delta u'$, $y' = y_0' + v'$, $\delta y = \delta v$ and $\delta y' = \delta v'$. At the equilibrium state, $x = x_0$ and $y = y_0$, then Eq. (28) can be simplified to

$$\delta \Pi = \delta \int_0^{Z_H} \left(T_a \sqrt{1 + x_0'^2 + y_0'^2} - F_u s_0' x_0 - F_v s_0' y_0 \right) dz_0 = 0 \tag{29}$$

This formulation is suitable and efficient for a practical cable problem of which the top tension is specified, the total cable arc-length either unstrained or strained is to be determined. Three unknowns to be involved in the algorithm are $x_0(z_0)$, $y_0(z_0)$ and $\varepsilon_0(z_0)$. The relevant equilibrium equation corresponding to the tangential direction of a cable segment (5a), representing the cable tension at any point, is converted to the following integral expression

$$T_a(z_0) = T_H - \int_{Z_0}^{Z_H} \left[\frac{w_e}{(1 + \varepsilon_0)} - D_p \sqrt{1 + x_0'^2 + y_0'^2} \right] dz_0 \tag{30}$$

in which T_H is the specified tension at the top end. The combination of Eqs. (29) and (30) are used to solve for the cable static problem.

Since the vertical axis is chosen as an independent variable, the total water depth is discretized into number of regions or elements, each with an equal length h as depicted in Fig. 3. In the analysis, the horizontal projection of element coordinates $x_0(z_0)$ and $y_0(z_0)$ on XZ and YZ planes consist of two components which are linear and non-linear. The linear parts (x_L, y_L) are directly obtained from the prescribed positions of cable while the non-linear parts (x_{NL}, y_{NL}) are approximated by a cubic polynomials shape function in z_0, thus

$$\begin{Bmatrix} x_{NL} \\ y_{NL} \end{Bmatrix} = [N]\{q\} \tag{31}$$
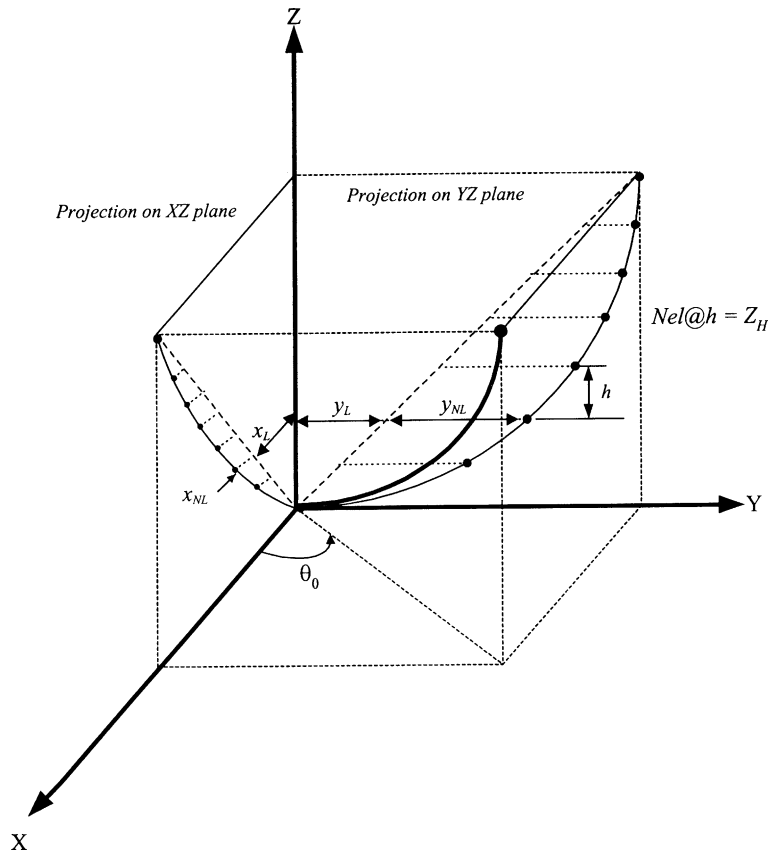

Fig. 3. Modelling for horizontal projection of the finite element coordinates on XZ and YZ planes.

where

$$[N] = \begin{bmatrix} N_1 & N_2 & 0 & 0 & N_3 & N_4 & 0 & 0 \\ 0 & 0 & N_1 & N_2 & 0 & 0 & N_3 & N_4 \end{bmatrix} \tag{32}$$

$$N_1 = 1 - 3(z_0^2/h^2) + 2(z_0^3/h^3), \quad N_2 = z_0 - 2(z_0^2/h) + (z_0^3/h^2)$$
$$N_3 = 3(z_0^2/h^2) - 2(z_0^3/h^3), \quad N_4 = -(z_0^2/h) + (z_0^3/h^2) \tag{33a–d}$$

$$\{q\} = \lfloor x_{\mathrm{NL}}(0) \quad x'_{\mathrm{NL}}(0) \quad y_{\mathrm{NL}}(0) \quad y'_{\mathrm{NL}}(0) \quad x_{\mathrm{NL}}(h) \quad x'_{\mathrm{NL}}(h) \quad y_{\mathrm{NL}}(h) \quad y'_{\mathrm{NL}}(h) \rfloor^{\mathrm{T}} \tag{34}$$

in which $[N]$ is the matrix of the shape function and $\{q\}$ is the degree of freedom of nodal displacement and rotation. For the kinematic relations of strain, the matrix notations can be written as

$$\varepsilon_0 = \lfloor L \rfloor \{e\} \tag{35}$$

$$\lfloor L \rfloor = \lfloor 1 - z_0/h \quad z_0/h \rfloor \tag{36}$$

$$\{e\} = \lfloor \varepsilon_0(0) \quad \varepsilon_0(h) \rfloor^{\mathrm{T}} \tag{37}$$

where $\lfloor L \rfloor$ is the matrix of the strain shape function and $\{e\}$ is the nodal strain. The global equilibrium condition $\delta\Pi = (\partial\pi/\partial q_i)\delta q_i = 0$ yields a system of non-linear equations. Consequently, by the Newton–Raphson iterative algorithm, one can write the incremental process as

$$[K]\{\Delta Q\} = -\{R\} \tag{38}$$

Consider the kth element, the contributions to the square matrix $[K]_k$ and to the vector $\{R\}_k$ are as follows,

$$[K]_k = \left[\frac{\partial^2 \pi_k}{\partial q_i \partial q_j}\right] = \int_0^h \frac{[N']^{\mathrm{T}} T_{\mathrm{a}}[N']}{(1 + x_0'^2 + y_0'^2)^{3/2}}\, \mathrm{d}z_0 \tag{39}$$

$$\{R\}_k = \left\{\frac{\partial \pi_k}{\partial q_i}\right\} = \int_0^h \left[\frac{[N']T_{\mathrm{a}}}{(1 + x_0'^2 + y_0'^2)^{1/2}}\begin{Bmatrix} x_0' \\ y_0' \end{Bmatrix} - [N]^{\mathrm{T}}\begin{Bmatrix} F_u \\ F_v \end{Bmatrix}\right] \mathrm{d}z_0 \tag{40}$$

in which h is an element height, $\{Q\}$ and $\{q\}$ are the global and local degrees of freedom, respectively. Eqs. (39) and (40) are evaluated by using Gaussian quadrature numerical integration with four points. The boundary conditions are the zero value of non-linear parts of coordinates at $z_0 = 0$ and Z_{H}. The step-by-step iteration procedure can be comprehensively described as follows:

- The initial estimated value of global strain $\{\Theta\}$ and global degrees of freedom $\{Q\}$ are assumed to be zero.
- The values of F_u, F_v and T_{a} are calculated consecutively.
- After the components of $[K]_k$ and $\{R\}_k$ are numerically evaluated, all element matrices are assembled together to form the global systems.
- By applying boundary conditions, the solutions of $\{\Delta Q\}$ are obtained using Eq. (38).
- The new value of nodal strain is updated by the Newton–Raphson process; that is, $\varepsilon^{n+1} = \varepsilon^n - f(\varepsilon^n)/f'(\varepsilon^n)$, in which $n = $ step of iteration,

$$f(\varepsilon_0^n) = EA\varepsilon_0^n + 2v\rho_w gA(1 - v\varepsilon_0^n)^2(Z_H - z_0) - T_H + \int_{Z_0}^{Z_H} \left[\frac{w_e}{(1 + \varepsilon_0^n)} - D_p\sqrt{1 + x_0'^2 + y_0'^2} \right] dz_0$$

and $f'(\varepsilon_0^n)$ is approximated using the forward difference formula; namely $f'(\varepsilon_0^n) = (f(\varepsilon_0^n + \Delta) - f(\varepsilon_0^n))/\Delta$. Since the spatial variation of the initial static strain of cable is very small compared to unity, the spatial step length used Δ is assumed to be a constant and it is set to be equal to 1×10^{-8}.

- Then an incremental global strain $\{\Delta\Theta\}$ is obtained.
- Adding an incremental global displacement $\{\Delta Q\}$ to Q and repeating overall steps, the iterative procedures are terminated when $\{\Delta Q\}$ and $\{\Delta\Theta\}$ are negligible or the error tolerance is achieved.

4.2. Shooting-optimization method

The following governing eight first-order differential equations, Eqs. (41)–(44), together with the eight known end conditions, Eq. (45) or (46), may be solved for T, θ, ϕ, x_0, y_0, s_0, s and ε_0 as functions of z_0. Let ξ_i, $i = 1, 2, \ldots, 8$ be the unknown parameters. In view of these governing equations and their associated initial conditions at the seabed, $z_0 = 0$, the preceding differential equations corresponding to the equilibrium of cable segment, Eq. (5), can be rearranged as follows

$$\frac{dT}{dz_0} = \left(\frac{w_e}{(1 + \varepsilon_0)} - \frac{D_p}{\sin\phi} \right), \quad T(0) = \xi_1$$

$$\frac{d\theta}{dz_0} = \left(-\frac{D_q}{T\cos\phi\sin\phi} \right), \quad \theta(0) = \xi_2 \tag{41a,b,c}$$

$$\frac{d\phi}{dz_0} = \left(\frac{w_e\cos\phi}{(1 + \varepsilon_0)} - D_r \right) \Big/ T\sin\phi, \quad \phi(0) = \xi_3$$

Differentiation of Eq. (6) with respect to z_0 gives

$$\frac{d\varepsilon_0}{dz_0} = \frac{dT/dz_0 + 2v\rho_w gA(1 - v\varepsilon_0)^2}{\{EA - 4v^2\rho_w gA(1 - v\varepsilon_0)(Z_H - z_0)\}}, \quad \varepsilon(0) = \xi_4 \tag{42}$$

From the geometrical considerations, Eqs. (7a)–(7c) can be rewritten as

$$\frac{dx_0}{dz_0} = \left(\frac{\cos\phi\cos\theta}{\sin\phi} \right), \quad x_0(0) = 0$$

$$\frac{dy_0}{dz_0} = \left(\frac{\cos\phi\sin\theta}{\sin\phi} \right), \quad y_0(0) = 0 \tag{43a,b,c}$$

$$\frac{ds_0}{dz_0} = \left(\frac{1}{\sin\phi} \right), \quad s_0(0) = 0$$

Finally, from the strain definition, Eq. (9a) can also be rewritten as

$$\frac{ds}{dz_0} = \left(\frac{1}{\sin\phi(1 + \varepsilon_0)} \right), \quad s(0) = 0 \tag{44}$$

The terminal boundary conditions depend on whether the top tension force or the unstrained cable length is specified, namely, for the case of specified top tension,

$$\theta(z_H) = \zeta_5, \quad \phi(z_H) = \zeta_6, \quad s_0(z_H) = \zeta_7, \quad s(z_H) = \zeta_8$$

$$T(z_H) = T_H, \quad x_0(z_H) = R\cos\theta_0, \quad y_0(z_H) = R\sin\theta_0, \quad \varepsilon_0(z_H) = \frac{T_H}{EA} \tag{45a–h}$$

for the case of specified cable unstrained length,

$$\theta(z_H) = \zeta_5, \quad \phi(z_H) = \zeta_6, \quad s_0(z_H) = \zeta_7, \quad s(z_H) = S_L$$

$$T(z_H) = \zeta_8, \quad x_0(z_H) = R\cos\theta_0, \quad y_0(z_H) = R\sin\theta_0, \quad \varepsilon_0(z_H) = \frac{\zeta_8}{EA} \tag{46a–h}$$

Instead of solving a set of algebraic equations formed from the error between the prescribed and computed terminal boundary values, the error norms are minimized by an optimization algorithm. The numerical procedure starts from the initial estimated values of T, θ, ϕ and ε at the bottom end. Then, the integration is carried out from $z_0 = 0$ to $z_0 = Z_H$ using the fifth-order Cash–Karp Runge–Kutta method as given in Press et al. [15]. An objective function Ψ for the optimization exercise is minimized using the downhill simplex method proposed by Nelder and Meade [16], depending on the specified values, namely, for the case of specified top tension,

$$\underset{x_0,y_0,T}{\text{Minimize}} \, \Psi = |x_0(Z_H) - R\cos\theta_0| + |y_0(Z_H) - R\sin\theta_0| + |T(Z_H) - T_H| \tag{47}$$

or for the case of specified cable unstrained length,

$$\underset{x_0,y_0,s}{\text{Minimize}} \, \Psi = |x_0(Z_H) - R\cos\theta_0| + |y_0(Z_H) - R\sin\theta_0| + |s(Z_H) - S_L| \tag{48}$$

Consequently, the overall steps are iterated until the allowable error is achieved. It should be remarked that the integration with respect to z_0 coordinate (from the seabed to the surface) has an implicit constraint that cable profile must lie above the seabed.

5. Computational results and discussion

Three case studies for some typical problems are presented. The first case provides confirmation of the accuracy of the variational formulation. The finite element method (FEM) and the shooting-optimization method (SOM) have been cross-checked for the validity of the cable model and mathematical examinations. The latter two cases consider the static behavior of cable, using the specified top tension or cable unstrained length to be the main type of analyses.

The cable data input parameters are as follows: $Z_H = 500$ m; $R = 300$ m; uniform current velocity in X-axis direction $V = 3.7$ km/h; cable diameter $D = 0.023$ m; weight of cable in seawater $w_e = 12.3$ N/m; $C_{DN} = 1.0$; $C_{DT} = 0.05$; $\rho_w = 1021$ kg/m^3, and $E = 0.1628 \times 10^7$ kN/m^2, and $v = 0$. The specified unstrained arc-length is 550 m and the specified top tension is 25 kN.

Numerical results given in Tables 1 and 2 show the cable tension components corresponding to the global directions at the bottom end and the cable strained length S_{L_0} versus the variations in values of θ_0 from 0° to 180°, for the case of specified top tension and cable unstrained length, respectively. The calculated length of S_{L_0} is equal to $\sum_{k=1}^{N_{el}} \int_0^h \sqrt{1 + x_0'^2 + y_0'^2} \, dz_0$, in which N_{el} is the

Table 1

Comparisons of cable tension components at the bottom end and cable strained length for the specified top tension case, FEM: finite element method, SOM: shooting-optimization method

θ_0 (deg)	Cable tension components at the buggy end						Strained length	
	T_x (N)		T_y (N)		T_z (N)		S_{L_0} (m)	
	FEM	SOM	FEM	SOM	FEM	SOM	FEM	SOM
0	13 044.77	13 044.82	0.00	0.00	13 917.31	13 917.26	587.18	587.18
30	11 860.48	11 860.42	5175.70	5175.96	14 004.11	14 004.06	587.26	587.26
60	8495.60	8495.53	9168.76	9168.88	14 379.29	14 379.25	587.21	587.21
90	3421.33	3421.33	11 057.45	11 057.49	15 122.85	15 122.82	586.44	586.44
120	−2401.31	−2401.30	10 051.88	10 051.10	15 986.69	15 986.68	584.99	584.99
150	−7179.69	−7179.69	5986.84	5986.84	16 565.44	16 565.43	583.71	583.71
180	−9024.86	−9024.87	0.00	0.00	16 735.33	16 735.32	583.25	583.25

Table 2

Comparisons of cable tension components at the bottom end and cable strained length for the specified cable unstrained arc-length case, FEM: finite element method, SOM: shooting-optimization method

θ_0 (deg)	Cable tension components at the buggy end						Strained length	
	T_x (N)		T_y (N)		T_z (N)		S_{L_0} (m)	
	FEM	SOM	FEM	SOM	FEM	SOM	FEM	SOM
0	23 641.42	23 641.38	0.00	0.00	31 267.32	31 267.22	584.16	584.16
30	21 078.43	21 078.44	10 398.89	10 398.83	31 397.11	31 397.05	584.19	584.19
60	13 875.21	13 875.27	18 226.10	18 226.12	31 798.84	31 798.88	584.18	584.18
90	3525.51	3525.50	21 387.09	21 387.02	32 344.99	32 344.86	584.00	584.00
120	−7370.06	−7370.05	18 747.21	18 747.21	32 752.48	32 752.43	583.62	583.62
150	−15 613.49	−15 613.50	10 871.71	10 871.72	32 895.07	32 895.07	583.27	583.27
180	−18 671.59	−18 671.58	0.00	0.00	32 905.56	32 905.52	583.14	583.14

number of elements used in FEM. This study used 20 elements in the calculation. It is seen that both methods yield almost identical results. In spite of the fact that on convergence of SOM is limited by an initial estimated condition, this method is efficient and robust, especially when the initial estimate is close to the solution. The solution of FEM is based on the total number of prescribed elements, whereas the solution of SOM is based on an adaptive step-size controlled by an algorithm in the Runge–Kutta process. To gain further insights into the cable static behavior, the following examples for various cable geometrical parameters are studied. For the sake of convenience, the following dimensionless quantities are introduced as an extensibility index, namely T_H/EA and $w_e S_L/EA$.

5.1. Specified top tension case

In this case, it was known that the maximum and minimum tensions occur at the cable top and bottom ends respectively, and the tension distribution is a function of ocean depth. A preliminary numerical investigation was carried out to demonstrate the effect of axial extensibility, using the

forgoing input data and FEM. The parameter of T_H/EA, fixed in value of top tension and cable diameter, is assumed to be equal to 1.0, 0.1, 0.01, 0.001 and 0.0001. The value of elastic modulus was varied considerably so that the extensibility effect can be clearly seen, and a value of prescribed angle θ_0 was also varied so that the significance of omnidirectional current actions is involved by maintaining the uniform current profile in the X-axis direction.

Fig. 4a–c illustrate the distribution of cable tension components corresponding to the global directions at the bottom end in each value of T_H/EA under the variations of θ_0 from 0° to 180°. It can be seen that the changes in a value of θ_0 and cable extensibility have effect on the tension in each direction as well as the resultant forces, namely $T_b = \sqrt{T_x^2 + T_y^2 + T_z^2}$, as shown numerically in Table 3. The tension T_b decreases with the decreasing values of T_H/EA and with the increasing values of θ_0. This tension is the important parameter in designing a cable and is capable of prediction to the cable sag condition [1,9].
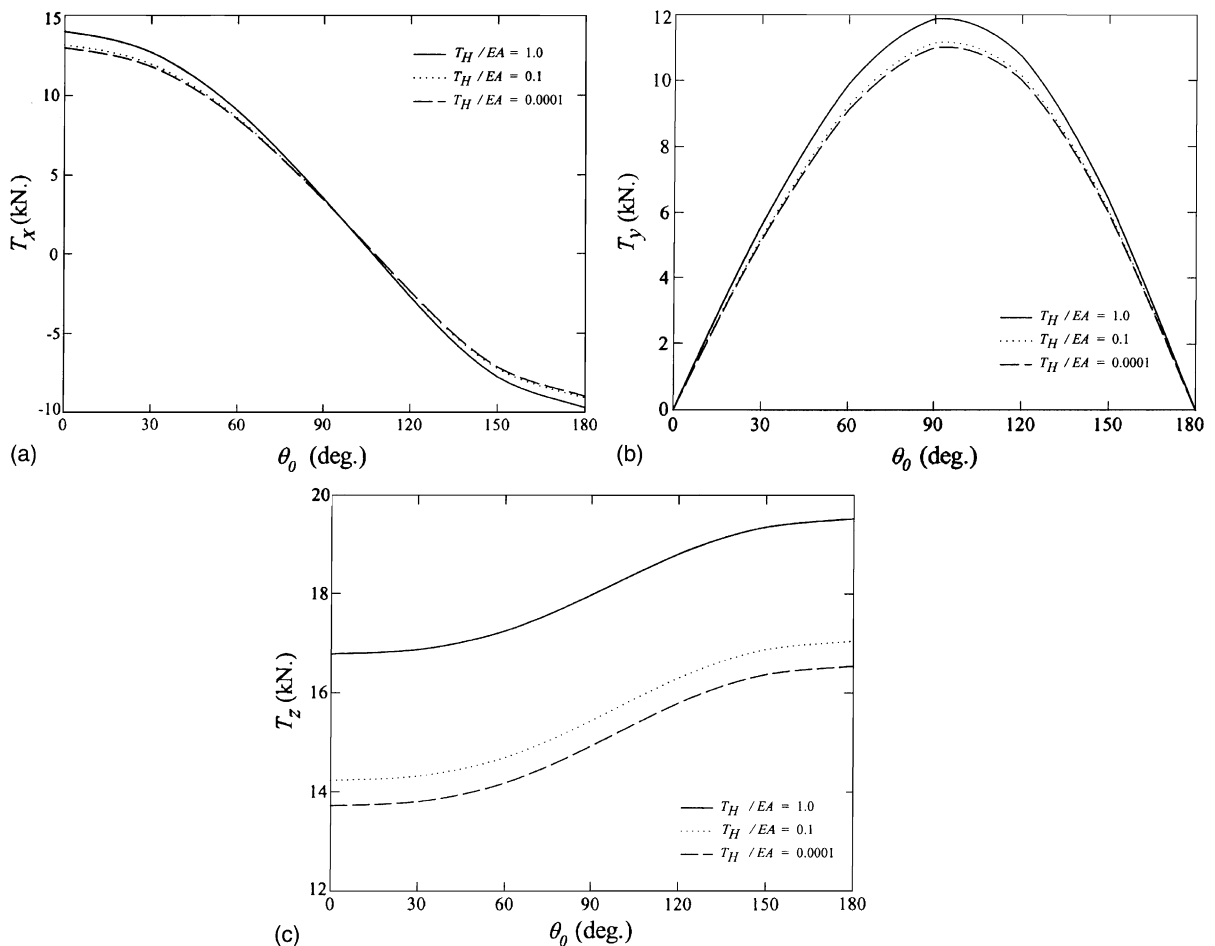
Fig. 4. Variation in tension components at the bottom end in each value of T_H/EA, for a different value of angle θ_0, for the specified top tension case: (a) tension in X-axis direction, (b) tension in Y-axis direction and (c) tension in Z-axis direction.

Table 3
Calculated values of the resultant forces at the bottom end and cable unstrained length in each value of T_H/EA, for the specified top tension case

θ_0 (deg)	$T_H/EA = 1.0$		$T_H/EA = 0.1$		$T_H/EA = 0.01$		$T_H/EA = 0.001$		$T_H/EA = 0.0001$	
	T_b (N)	S_L (m)	T_b (N)	S_L (m)	T_b (N)	S_L (m)	T_b (N)	S_L (m)	T_b (N)	S_L (m)
0	21 855.66	301.77	19 382.31	539.06	18 934.62	582.13	18 886.46	586.77	18 881.61	587.23
30	21 848.02	302.06	19 374.84	539.21	18 927.20	582.23	18 879.05	586.86	18 874.20	587.33
60	21 832.78	302.54	19 359.85	539.29	18 912.32	582.19	18 864.18	586.81	18 859.32	587.27
90	21 824.19	302.50	19 351.14	538.64	18 903.60	581.40	18 855.46	586.00	18 850.61	586.47
120	21 815.76	302.27	19 342.98	537.41	18 895.53	579.94	18 847.40	584.51	18 842.55	584.97
150	21 800.52	302.25	19 328.14	536.38	18 880.84	578.65	18 832.73	583.20	18 827.88	583.66
180	21 792.84	302.30	19 320.62	536.03	18 873.38	578.19	18 825.27	582.73	18 820.42	583.18

In each value of T_H/EA, the calculated unstrained length of S_L equal to $\sum_{k=1}^{N_{el}} \int_0^h \sqrt{1 + x_0'^2 + y_0'^2/(1 + \varepsilon_0)}\, dz_0$ is not quite different under the variations of θ_0. The shortest length can be found when cable having high extensible cable ($T_H/EA = 1.0$), however, the length is increased under high elongation and almost equal to the lower one at the equilibrium state, as shown in Fig. 5. The effect of extensibility on the cable unstrained and strained length can be clearly seen when T_H/EA is greater than 0.1. The shortest strained length may be approximated when θ_0 is equal to 180°.

The next investigation was to consider the cable orientation under the influence of current time-independent forces, in terms of magnitude and direction. Three values of velocity were considered, V is taken to have value of 0, 2.0, 3.7 km/h, and T_H/EA was taken to be 0.1. Figs. 6 and 7 present the distributions of vertical angle ϕ and horizontal angle θ against the ocean depth under the variations of θ_0 for any nodal point along the cable, where ϕ is measured from XY plane and θ is
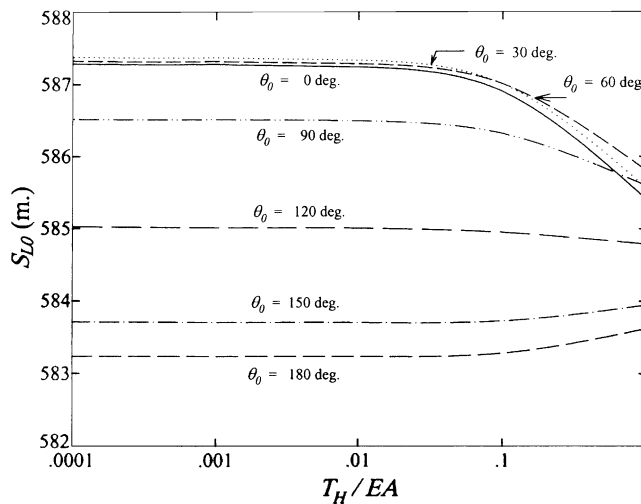

Fig. 5. Variation in total cable strained length in each value of angle θ_0, for a different value of T_H/EA, for the specified top tension case.
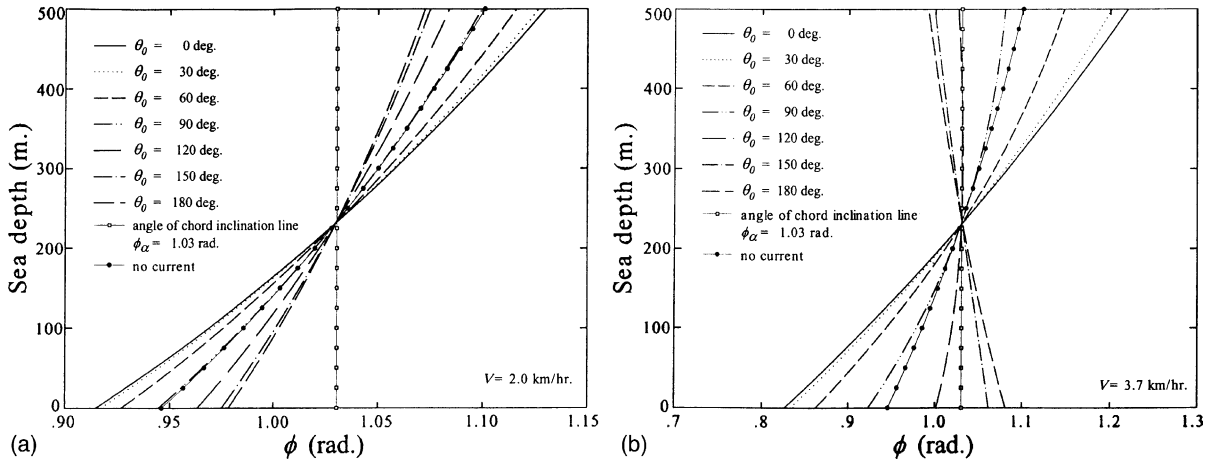
Fig. 6. Distribution of vertical angle ϕ at any point along a cable against ocean depth, for a different value of angle θ_0, for the specified top tension case and $T_H/EA = 0.1$: (a) $V = 2.0$ km/h and (b) $V = 3.7$ km/h.
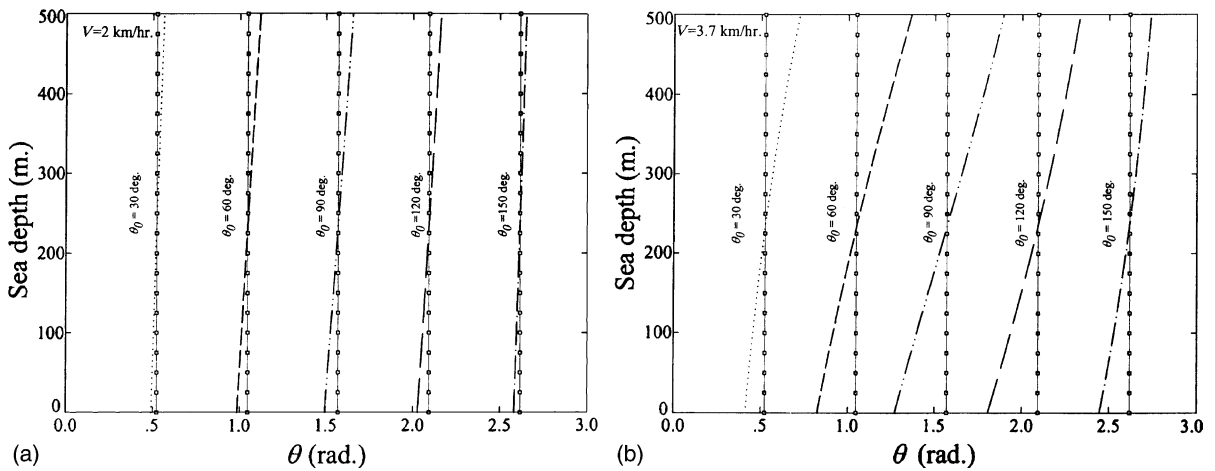

Fig. 7. Distribution of horizontal angle θ at any point along a cable against ocean depth, for a different value of angle θ_0, for the specified top tension case and $T_H/EA = 0.1$: (a) $V = 2.0$ km/h and (b) $V = 3.7$ km/h (—□—: no current).

measured from the $\vec{i}$ direction. These illustrations are useful for evaluating the cable equilibrium profile in space with the different action of current forces instead of cable sag prediction.

As shown in Fig. 6a for $V = 2.0$ km/h, the distribution of ϕ is varied along the depth, and the values of ϕ at the top and bottom ends are respectively greater and less than the value of ϕ_α. For $\theta_0 = 0°$, it may be speculated that cable is more slack than the others since values of ϕ are maximum and minimum at the top and bottom ends, respectively. When $\theta_0 = 90°$, the plot is identical to the case of no current.

As shown in Fig. 6b, when the magnitude of V is increased to 3.7 km/h, the plots for θ_0 equal to 120°, 150° and 180° are different from the former case. For $\theta_0 = 120°$, the value of ϕ in the range

of 250–500 m depth aligns closely to the angle ϕ_α. Hence, the sag of cable is apparently small for this situation. For $\theta_0 = 150°$ and $180°$, the values of ϕ at the top and bottom ends are respectively less and greater than ϕ_α. Therefore, the profiles are formed in the contrary direction with respect to a normal shape of the other prescribed angles θ_0. This feature may be explained as current forces in the lateral direction having a more significant influence on the cable configuration more than the cable effective self-weight. This effect becomes significance especially as the magnitude of V increases.
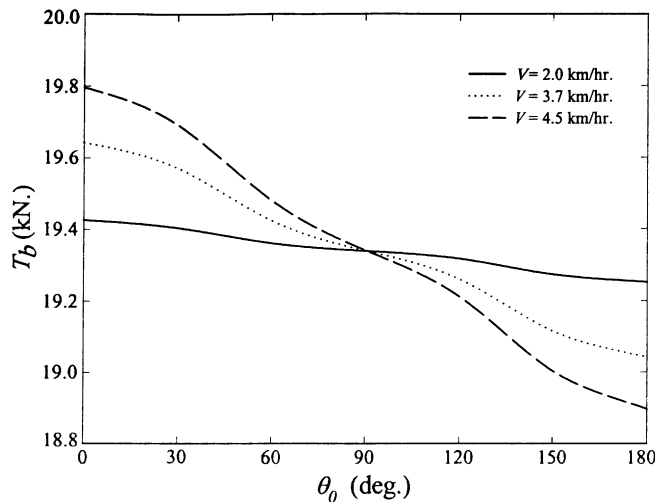
Fig. 8. Variation in the resultant forces at the bottom end in each current magnitude, for a different value of angle θ_0, for the specified top tension case and $T_H/EA = 0.1$.
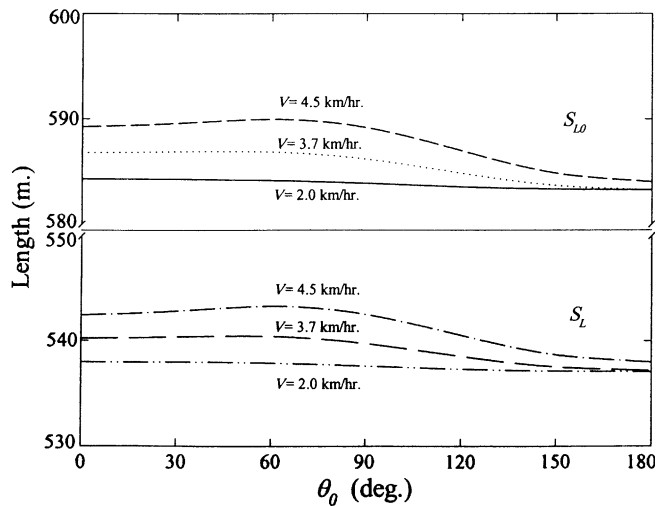

Fig. 9. Variation of cable strained and unstrained lengths in each current magnitude, for a different value of angle θ_0, for the specified top tension case and $T_H/EA = 0.1$.

Fig. 7a presents how the current forces displace the cable laterally, which is more noticeable with the higher magnitude of the current velocity, as compared with Fig. 7b. The vertical lines in the plots are used to represent for the absence of currents in each specified value of θ_0. It may be seen that cable configuration entirely lies in the vertical plane because there is no force to disturb the cable from the plane, as is well-known for the case of a submerged cable. For $\theta_0 = 0°$ and $180°$ (not shown herein), the current direction is parallel to the cable configuration line, therefore the force component in the bi-normal direction ($\vec{q}$) is not generated. This makes a cable lies in the vertical plane and only in the distribution of vertical angle has been presented in Fig. 6.

Fig. 8 shows the influence of changes in the magnitude of current velocity on the resultant forces at the bottom end in each value of θ_0. It can be seen that, for the ranges of $0° < \theta_0 < 90°$ and $90° < \theta_0 < 180°$, respectively, tension T_b increases and decreases with the increasing magni-

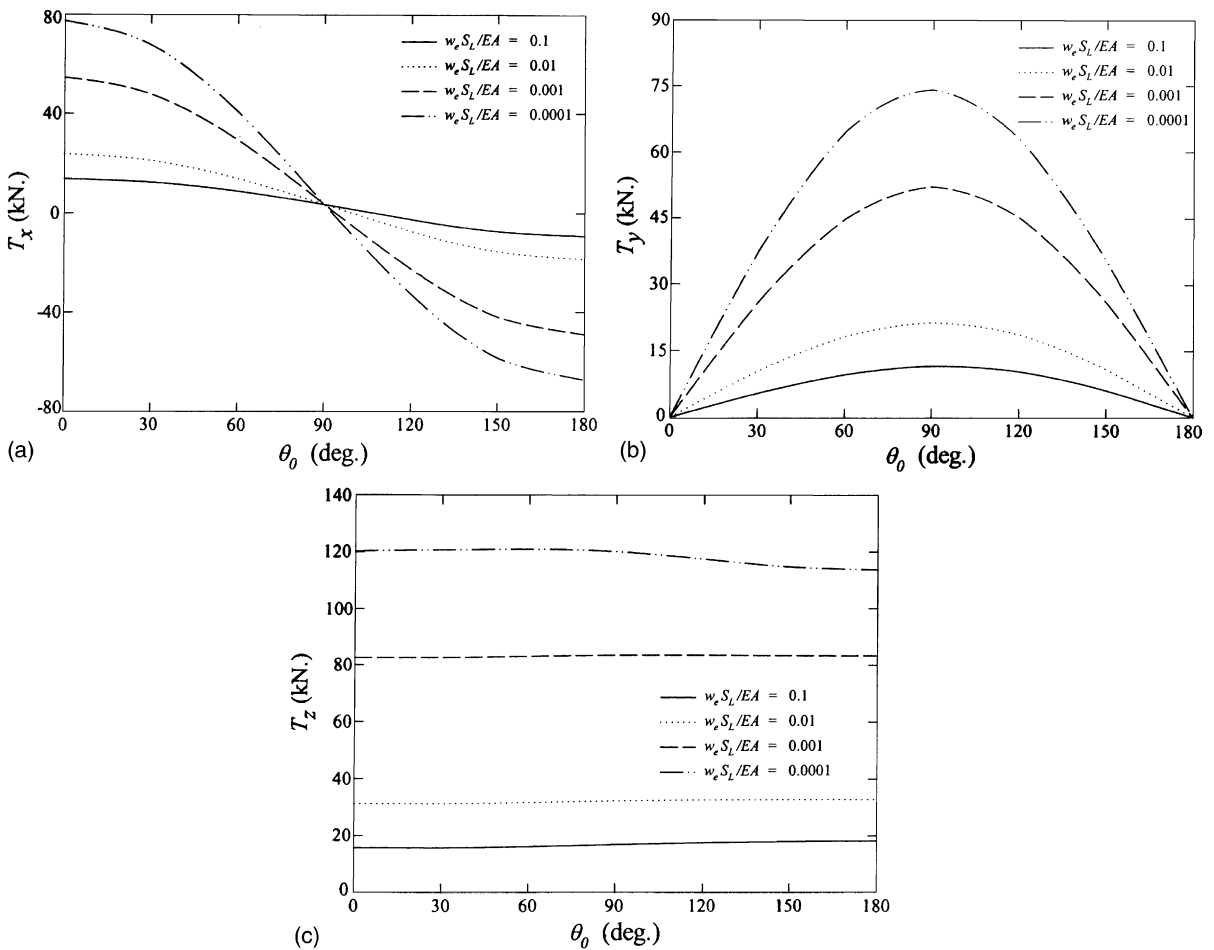Fig. 10. Variation in tension components at the bottom end in each value of $w_e S_L/EA$, for a different value of angle θ_0, for the specified cable unstrained arc-length case: (a) tension in X-axis direction, (b) tension in Y-axis direction and (c) tension in Z-axis direction.

tude of current velocity. Moreover, the cable strained and unstrained lengths increase with the increasing magnitude of current velocity, as presented in Fig. 9.

5.2. Specified unstrained arc-length case

Although the numerical algorithm mentioned above is efficient for solving the cable problem with the case of specified top tension, this algorithm can be treated using the concept of specified unstrained length. Firstly, the initial trial value of top tension is assigned, and then the approximated unstrained length is calculated. If the computed length is not equal to the prescribed one, then a new trial value of tension will be assumed and the procedure is repeated until the allowable error is achieved.

Table 4
Calculated values of the resultant forces at the bottom and top ends in each value of w_eS_L/EA, for the specified cable unstrained arc-length case

| θ_0 (deg)	$w_eS_L/EA = 0.1$		$w_eS_L/EA = 0.01$		$w_eS_L/EA = 0.001$		$W_eS_L/EA = 0.0001$	
	T_b (N)	T_H (N)	T_b (N)	T_H (N)	T_b (N)	T_H (N)	T_b (N)	T_H (N)
0	21 403.77	25 337.52	39 897.99	45 390.63	99 605.96	105 368.65	142 913.56	148 750.00
30	21 374.50	25 372.05	39 881.10	45 447.08	99 609.28	105 153.04	142 838.37	148 750.00
60	21 291.62	25 418.22	39 774.90	45 488.28	99 492.51	105 479.74	142 687.98	148 750.00
90	21 172.94	25 374.98	39 483.72	45 275.88	99 027.31	105 090.33	140 737.33	146 875.00
120	21 014.82	25 292.22	38 987.38	44 858.40	98 182.48	104 321.29	137 302.34	143 515.63
150	20 837.21	25 248.79	38 491.45	44 512.63	97 375.51	103 664.55	133 401.68	139 765.63
180	20 762.51	25 240.96	38 398.26	44 394.38	97 068.48	103 432.62	131 920.12	138 359.38
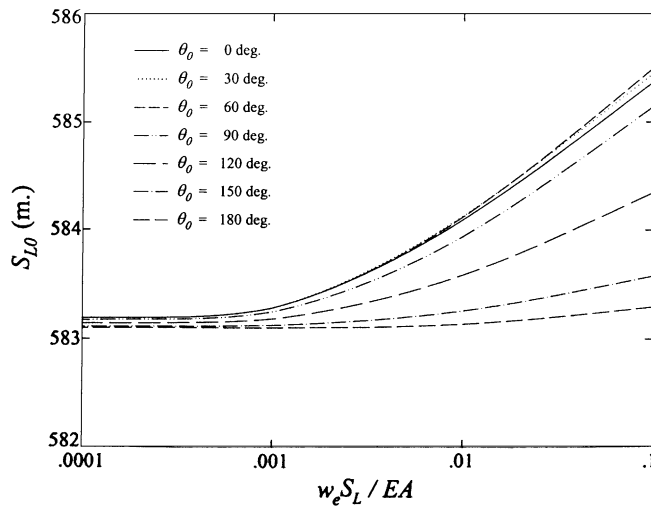
Fig. 11. Variation in total cable strained length in each value of angle θ_0, for a different value of w_eS_L/EA, for the specified cable unstrained arc-length case.

In accordance with the representation of specified top tension case, the following results are shown to demonstrate the effect of extensibility and the omnidirectionality of current forces. By assuming a parameter of $w_e S_L/EA = 0.1, 0.01, 0.001, 0.0001$, the value of w_e/A is kept constant, whereas the specified cable unstrained length S_L is equal to 400, 550, 575 and 582 m, and the corresponding cable elastic modulus E is equal to 0.118×10^6, 0.163×10^7, 0.170×10^8, 0.172×10^9 kN/m^2, respectively. Once again, Fig. 10a–c illustrate the distributions of cable tension components at the bottom end in each value of $w_e S_L/EA$ and under the variations of θ_0 from 0° to 180°. It can be clearly seen that the changes in a value of θ_0 and cable extensibility have effects on the tension in each direction and also on the resulting force T_b, which decreases consecutively from
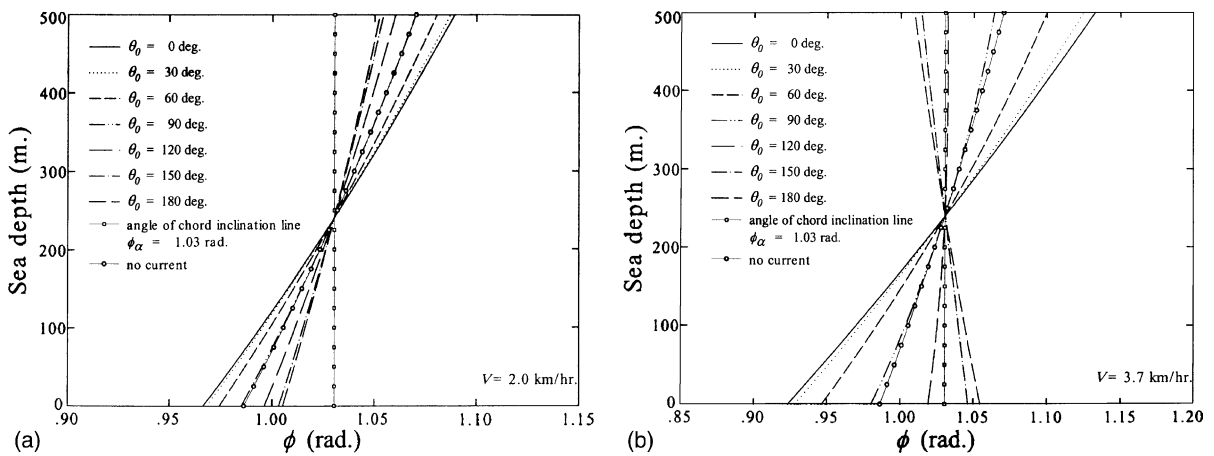

Fig. 12. Distribution of vertical angle ϕ at any point along a cable against ocean depth, for a different value of angle θ_0, for the specified cable unstrained arc-length case and $w_e S_L/EA = 0.01$: (a) $V = 2.0$ km/h and (b) $V = 3.7$ km/h.
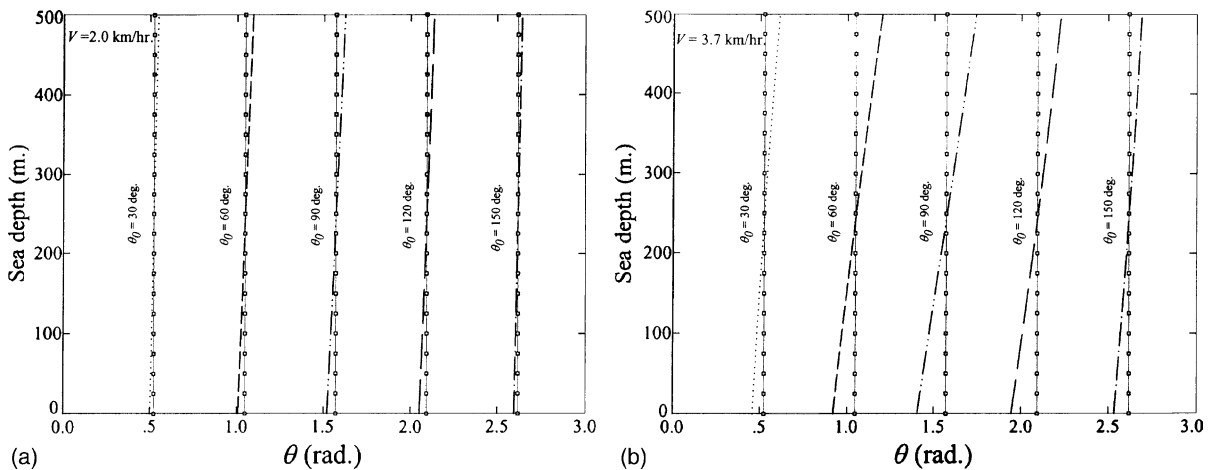

Fig. 13. Distribution of horizontal angle θ at any point along a cable against ocean depth, for a different value of angle θ_0, for the specified cable unstrained arc-length case and $w_e S_L/EA = 0.01$: (a) $V = 2.0$ km/h and (b) $V = 3.7$ km/h (—□—: no current).

$\theta_0 = 0°$ to $180°$, as shown in Table 4. In each value of $w_e S_L/EA$, the maximum required top tension T_H can be found when $\theta_0 = 60°$, approximately.

Fig. 11 shows the computed cable strained length for each angle θ_0. It is worth noticing that these strained lengths are comparable (in the range of 583–586 m), even though the specified unstrained cable lengths are quite different (400–582 m) for each value of $w_e S_L/EA$. This can be explained that the highly extensible (small E) cable with shorter length can be stretched considerably more than that of the low extensible (large E) cable with longer length. Figs. 12 and 13 are
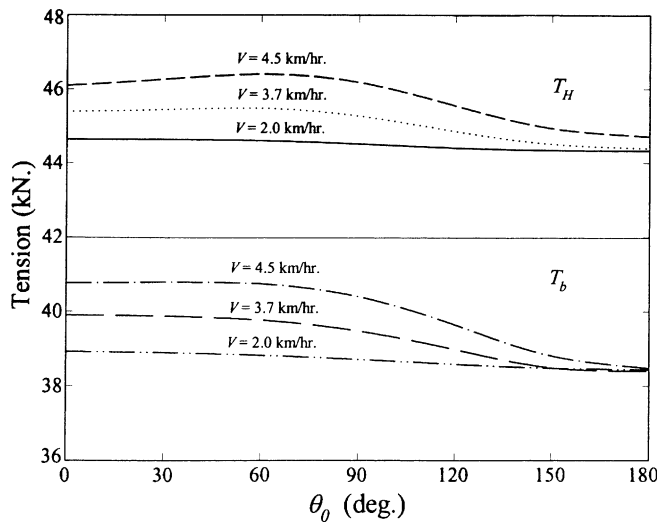

Fig. 14. Variation in the resultant forces at the top and bottom ends in each current magnitude, for a different value of angle θ_0, for the specified cable unstrained arc-length case and $w_e S_L/EA = 0.01$.
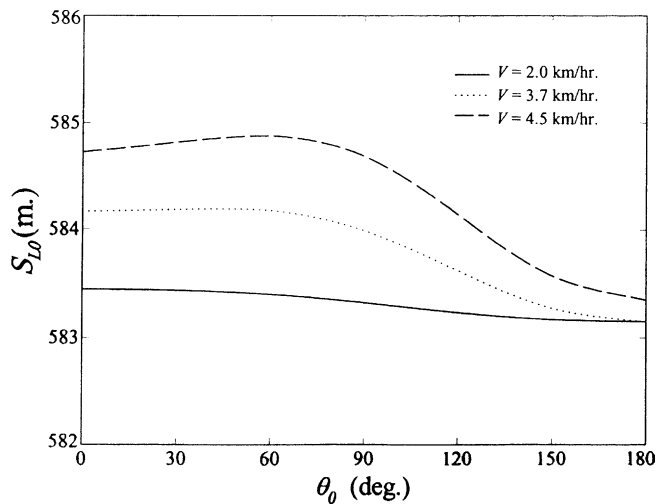

Fig. 15. Variation of cable strained length in each current magnitude, for a different value of angle θ_0, for the specified cable unstrained arc-length case and $w_e S_L/EA = 0.01$.

plotted to show the distribution of ϕ and θ for $w_e S_L / EA = 0.01$, under the variation in magnitude and direction of current velocity. It can be seen that the results in these figures are in good agreement with those in the aforementioned case. Fig. 14 shows the effect of current on the resultant forces at the top and bottom ends under the variation in value of θ_0. The results show that tensions T_H and T_b increase with the increasing magnitude of current velocity as well as the strained length, as shown in Fig. 15.

6. Conclusions

The variational model formulation and computational results for analyzing the three-dimensional steady-state behavior of an extensible marine cable is presented. Two mathematical simulations were used to solve and evaluate the problems, namely, the finite element approach and the shooting-optimization procedure, which gave almost identical results. The cable model and algorithm technique proposed in this study is efficient and robust when the top tension is specified. Numerical investigations were carried out for the specified top tension case and specified cable unstrained arc-length case. A number of parametric studies have been presented to evaluate cable profile, the tensile force development and the cable length estimation. The combined effects of axial extensibility and the current forces, both in terms of magnitude and directions, have been shown to be significant on the static behavior of extensible marine cable.

Acknowledgements

References

[1] A.P.K. De Zoysa, Steady-state analysis of undersea cables, Ocean Engineering 5 (1978) 209–223.
[2] S. Chucheepsakul, S. Subwonglee, Three-dimensional static analysis of marine cables, in: Cheung, Lee, Leung (Eds.), Computational Mechanics, Balkema, Rotterdam, Netherlands, 1991, pp. 389–394.
[3] C.M. Wang, H.F. Cheong, S. Chucheepsakul, Static analysis of marine cables via shooting-optimization technique, Journal of Waterway, Port, Coastal and Ocean Engineering ASCE 119 (1993) 450–457.
[4] M.I. Friswell, Steady-state analysis of underwater cables, Journal of Waterway, Port, Coastal and Ocean Engineering ASCE 121 (1995) 98–104.
[5] R.W. Webster, Nonlinear static and dynamic response of underwater cable structures using finite element method, in: Proceeding of the 7th Offshore Technology Conference ASCE 1975, Paper OTC 2322, Houston, Texas.
[6] L. Huyse, M.C. Singh, M.A. Maes, A static drilling riser model using free boundary conditions, Ocean Engineering 24 (1997) 431–444.
[7] T.P. Dreyer, J.H. Van Vuuren, A comparison between continuous and discrete modelling of cables with bending stiffness, Applied Mathematical Modelling 23 (1999) 527–541.
[8] D. Vassalos, Physical modelling and similitude of marine structures, Ocean Engineering 26 (1999) 111–123.
[9] M.A. Vaz, M.H. Patel, Three-dimensional behaviour of elastic marine cables in sheared currents, Applied Ocean Research 22 (2000) 45–53.

[10] S. Chucheepsakul, T. Huang, P. Laohaporjanart, Effect of axial deformation on the equilibrium configurations of marine cables, in: Proceeding of the 5th International Journal of Offshore and Polar Engineering Conference 1995, vol. 2, pp. 244–248.

[11] H.O. Berteaux, Buoy Engineering, John Wiley and Sons, New York, 1976, pp. 97–134.

[12] T.R. Goodman, J.P. Breslin, Statics and dynamics of anchoring cable in waves, Journal of Hydronautics 10 (1976) 113–120.

[13] C.P. Sparks, The influence of tension, pressure and weight on pipe and riser deformations and stresses, Journal of Energy Resource Technology ASME 106 (1984) 46–54.

[14] J.J. Burgess, Bending stiffness in a simulation of undersea cable deployment, International Journal of Offshore and Polar Engineering 3 (1993) 197–204.

[15] W.H. Press, S.A. Teukolsky, W.T. Vettering, B.P. Flannery, Numerical Recipes in Fortran, second ed., Cambridge University Press, Cambridge, 1992, pp. 372–381, 708–716.

[16] J.A. Nelder, R. Meade, A simplex method for function minimization, Computer Journal 7 (1965) 308–313.